

Phosphoregulation promotes release of kinetochores from dynamic microtubules via multiple mechanisms

Krishna K. Sarangapani^a, Bungo Akiyoshi^{b,c,1}, Nicole M. Duggan^b, Sue Biggins^b, and Charles L. Asbury^{a,2}

^aDepartment of Physiology and Biophysics, and ^cMolecular and Cellular Biology Program, University of Washington, Seattle, WA 98195; and ^bDivision of Basic Sciences, Fred Hutchinson Cancer Research Center, Seattle, WA 98109

Edited by Don W. Cleveland, University of California at San Diego, La Jolla, CA, and approved March 25, 2013 (received for review November 28, 2012)

During mitosis, multiprotein complexes called kinetochores orchestrate chromosome segregation by forming load-bearing attachments to dynamic microtubule tips, and by participating in phosphoregulatory error correction. The conserved kinase Aurora B phosphorylates the major microtubule-binding kinetochore subcomplexes, Ndc80 and (in yeast) Dam1, to promote release of erroneous attachments, giving another chance for proper attachments to form. It is unknown whether Aurora B phosphorylation promotes release directly, by increasing the rate of kinetochore detachment, or indirectly, by destabilizing the microtubule tip. Moreover, the relative importance of phosphorylation of Ndc80 vs. Dam1 in the context of whole kinetochores is unclear. To address these uncertainties, we isolated native yeast kinetochore particles carrying phosphomimetic mutations on Ndc80 and Dam1, and applied advanced laser-trapping techniques to measure the strength and stability of their attachments to individual dynamic microtubule tips. Rupture forces were reduced by phosphomimetic mutations on both subcomplexes, in an additive manner, indicating that both subcomplexes make independent contributions to attachment strength. Phosphomimetics on either subcomplex reduced attachment lifetimes under constant force, primarily by accelerating detachment during microtubule growth. Phosphomimetics on Dam1 also increased the likelihood of switches from microtubule growth into shortening, further promoting release in an indirect manner. Taken together, our results suggest that, in vivo, Aurora B releases kinetochores via at least two mechanisms: by weakening the kinetochore-microtubule interface and also by destabilizing the kinetochore-attached microtubule tip.

Kinetochores are large protein assemblies consisting of ~seven core subcomplexes (>50 different proteins) arranged hierarchically on centromeric DNA to form a multivalent microtubule-binding interface (1–3). The most fundamental activity of kinetochores is coupling mitotic or meiotic chromosomes to the growing and shortening tips of spindle microtubules. Kinetochore also participate in a vital surveillance mechanism that detects when erroneous kinetochore-microtubule attachments have formed, and releases these erroneous attachments via the action of Aurora B kinase. If Aurora B is inhibited, improper attachments accumulate and the accuracy of mitosis is severely compromised (4–7).

At their core, kinetochores contain three microtubule-binding elements, referred to in yeast as the Ndc80, Spc105, and Dam1 subcomplexes. Ndc80 and Spc105 are part of the widely conserved KMN network that is essential for kinetochore-microtubule coupling across eukaryotes (1, 2, 8). The yeast-specific Dam1 subcomplex, and a possible functional homolog in higher eukaryotes, the Ska1 subcomplex, localizes to kinetochores in a manner that depends on the presence of the Ndc80 subcomplex (9, 10). Purified Dam1 or Ndc80 subcomplexes alone form persistent, load-bearing attachments to dynamic microtubule tips in vitro (11–15). Purified Dam1 and Ndc80 subcomplexes also interact together on microtubules, and the performance of Ndc80-based tip couplers is enhanced when free Dam1 subcomplex is added (16, 17). These observations suggest that both Ndc80 and Dam1

provide important points of contact between kinetochores and microtubules.

The heteromultimeric coupling of kinetochores to microtubules implies that Aurora B could promote kinetochore release in multiple ways. Phosphorylation could directly weaken kinetochore-microtubule bonds, or it could disrupt interactions between various elements within the kinetochore. Consistent with a direct weakening of kinetochore-microtubule bonds, purified Ndc80 and Dam1 subcomplexes exhibit lower affinities and faster detachment from taxol-stabilized microtubules when they are phosphorylated in vitro (8, 18, 19), or when they carry phosphomimetic mutations at known Aurora B target sites (20–22). In addition, phosphorylation of purified Dam1 subcomplex abolishes its microtubule-dependent interaction with purified Ndc80 (16, 17), and phosphomimetic mutations reduce the propensity for purified Dam1 to oligomerize into microtubule-encircling rings (23). These observations suggest that Aurora B may trigger a release of Dam1 from the kinetochore or an opening of the Dam1 ring. Although different molecular interfaces are implicated in each of these scenarios, phosphorylation in all of these cases is expected to immediately accelerate the rate of detachment of the kinetochore from the microtubule.

The idea that Aurora B phosphorylation immediately triggers kinetochore release is simple and attractive. However, this view is challenged by the observation that reactivating Aurora B in tissue culture cells, via washout of reversible inhibitors, did not trigger immediate release of erroneous kinetochore attachments (24). Instead the kinetochore-attached microtubules began to disassemble, carrying the kinetochores to the spindle pole, where the attachments were subsequently released and corrected by an unknown mechanism. In vitro experiments further suggest that Aurora B phosphorylation does more than simply accelerating detachment. Phosphomimetic mutations block the ability of purified human Ndc80 subcomplex to promote switches from microtubule shortening into growth (i.e., “rescues”) (21). Various reconstituted tip couplers, including those composed of Ndc80 and Dam1, and also native yeast kinetochore particles, all detach much more quickly from shortening than from growing microtubule tips (14, 25, 26). Thus, changes in microtubule switch rates that favor disassembly can strongly promote kinetochore release (Fig. 1A). Collectively these observations suggest that phosphorylation can also promote release indirectly, via destabilization of the microtubule tip.

Here we take an in vitro approach to understand how Aurora B promotes kinetochore release. Our method allows direct observation of kinetochore detachment from dynamic microtubule

Author contributions: K.K.S., B.A., N.M.D., S.B., and C.L.A. designed research; K.K.S., B.A., and N.M.D. performed research; B.A. and N.M.D. contributed new reagents/analytic tools; K.K.S. analyzed data; and K.K.S., S.B., and C.L.A. wrote the paper.

The authors declare no conflict of interest.

This article is a PNAS Direct Submission.

¹Present address: Sir William Dunn School of Pathology, University of Oxford, Oxford OX1 3RE, United Kingdom.

²To whom correspondence should be addressed. E-mail: casbury@u.washington.edu.

This article contains supporting information online at www.pnas.org/lookup/suppl/doi:10.1073/pnas.1220700110/-DCSupplemental.

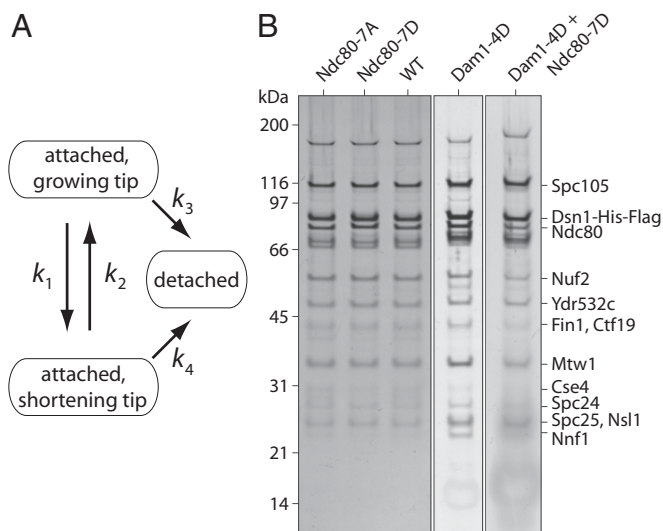


Fig. 1. Kinase phosphorylation can promote release of kinetochores from microtubules directly or indirectly. (A) The kinetochore-attached microtubule tip can grow (assemble) or shorten (disassemble), with transitions between these states governed by the rates of catastrophe, k_1 , and rescue, k_2 . The kinetochore can detach from either state, with rates k_3 and k_4 . Phosphorylation may promote release directly by accelerating the rates of detachment (k_3 or k_4). Because k_4 is generally much faster than k_3 (14, 25, 26), phosphorylation may also promote release indirectly by accelerating catastrophe (k_1) or inhibiting rescue (k_2). In principle, all four kinetic rates could be influenced by kinase phosphorylation. (B) The relative abundance of core kinetochore proteins that copurified with Dsn1-His-Flag was similar for wild-type (WT, SBY8524), Ndc80-7A (SBY8522), Ndc80-7D (SBY8523), Dam1-4D (SBY9021), and for the double-mutant, Ndc80-7D + Dam1-4D (SBY9020). Proteins were separated by SDS/PAGE and detected by silver staining. Additional mutants are shown in Fig. S1.

tips under conditions that closely match the physiological situation, and where tip dynamics can be simultaneously determined. With this capability we have begun to dissect the roles that phosphorylation at specific Aurora B target sites play in promoting kinetochore detachment.

Results

Purification of Phosphomimetic and Phospho-Deficient Kinetochore Particles. Kinetochore particles were purified from budding yeast strains carrying phosphomimetic mutations at previously identified Aurora B target sites. We focused on seven sites in the N-terminal “tail” of Ndc80 (threonines 21, 54, 71, and 74; serines 37, 95, and 100) (27), and four in the Dam1 protein of the Dam1 subcomplex (serines 20, 257, 265, and 292) (28), because prior work suggests that these sites are in or near key microtubule-binding interfaces (18, 20, 29–33) and that their phosphorylation is likely to affect microtubule attachment in vivo (22, 28, 29, 34–36). We prepared phosphomimetic mutants in which the targeted residues were mutated to aspartic or glutamic acid (single letter codes, D or E) to mimic constitutive phosphorylation. Whenever possible, we also prepared phospho-deficient controls, in which the same sites were mutated to alanine (single letter code, A) to mimic the unphosphorylated state.

Four kinetochore types were used extensively in our study (Tables S1–S5): Ndc80-7D, with the seven Ndc80 sites all mutated to aspartic or glutamic acid; Ndc80-7A, with the same sites all mutated to alanine; Dam1-4D, with the four Dam1 sites all mutated to aspartic acid; and a double mutant, Ndc80-7D + Dam1-4D, carrying both sets of phosphomimetic (aspartic or glutamic acid) substitutions. Cells carrying the *dam1-4D* allele, either alone or in combination with *ndc80-7D*, were viable but

grew extremely slowly, consistent with previous observations (28). We were not able to purify Dam1-4A kinetochores because *dam1-4A* cells were inviable, as previously reported (28). To specifically test the importance of serine 20 of Dam1, which has been implicated in phosphoregulation of Dam1-microtubule affinity (19), we included four additional kinetochore types, mainly in rupture force measurements (Table S1): Dam1-S20A and Dam1-S20D, with single substitutions at one of the four Dam1 sites, serine 20, plus Dam1-3A and Dam1-3D, with substitutions at the three remaining Dam1 sites (serines 257, 265, and 292). To further dissect the roles of Ndc80 and Dam1, we included two more double-mutants: Ndc80-7D + *dad1-1*, for which the seven phosphomimetic substitutions on Ndc80 were combined with a temperature-sensitive mutation of Dad1, a component of the Dam1 subcomplex, and Ndc80-7A + *dad1-1*, combining the latter with phospho-deficient Ndc80. Previous work suggests that the Dam1 subcomplex may be completely disrupted in *dad1-1* strains at the nonpermissive temperature (37).

Native kinetochore particles were isolated as previously described (25). Briefly, the Dsn1 component of the kinetochores was dual-tagged with Flag for purification and His₆ for linking to polystyrene beads (Materials and Methods and SI Materials and Methods). Affinity purification under physiological concentrations of salt yields stable, large assemblies that include the majority of core kinetochore subcomplexes except CBF3 (25). None of the phosphomimetic or phospho-deficient mutations caused major changes in the bulk composition of the purified kinetochore material, as determined by silver-stained SDS/PAGE (Fig. 1B and Fig. S1). We caution, however, that the intensity of silver-stained bands does not necessarily reflect stoichiometry within the particles measured in the laser trap. The Dam1 subcomplex, for example, is not abundant enough to be visible by silver staining, yet it clearly makes an important contribution to the coupling strength of individual particles (as shown below). We speculate that our laser-trap assay might select for a subset of particles retaining Dam1. Rigorously testing this idea will require the development of a method to simultaneously determine stoichiometry and tip-coupling strength at the single-particle level.

Measuring Kinetochore Particle Binding and Tip-Coupling Strength.

We linked kinetochore particles to 0.4- μ m diameter polystyrene beads, which served as artificial cargoes (in place of the chromosomes), and as handles for manipulating the kinetochores with a laser trap (25, 38). The density of kinetochore particles decorating the beads was adjusted by mixing 6-pM beads with different amounts of purified kinetochore material, corresponding to Dsn1 concentrations of 0.6–70 nM (Dsn1:bead ratios of 100:1–12,000:1). Kinetochore-decorated beads were introduced into a chamber containing dynamic microtubules growing from stable, coverslip-anchored seeds. The filaments exhibited dynamic instability typical of microtubules in vitro, switching stochastically between periods of slow growth and rapid shortening. To test for initial binding, candidate beads diffusing freely in solution were captured with the laser and held near the tips of growing filaments. When decorated at the highest kinetochore concentrations (65–70 nM Dsn1), most beads bound readily to the tips. However, as the decoration density was reduced, the fraction of active beads fell monotonically, with half-maximal binding typically occurring at \sim 6 nM Dsn1 (Fig. 2C and Table S1). The laser trap was controlled by a computer to apply precise tensile forces, in the direction of microtubule growth, to the tip-attached kinetochores (Fig. 24). To assess their strength, we operated the trap in a force-ramp mode, where the bead-trap separation was initially held constant (preload regime) (Fig. 2B) and then automatically increased at a constant rate until the kinetochore-microtubule attachment ruptured (ramp regime) (Fig. 2B). Rupture force distributions were recorded for populations of beads decorated

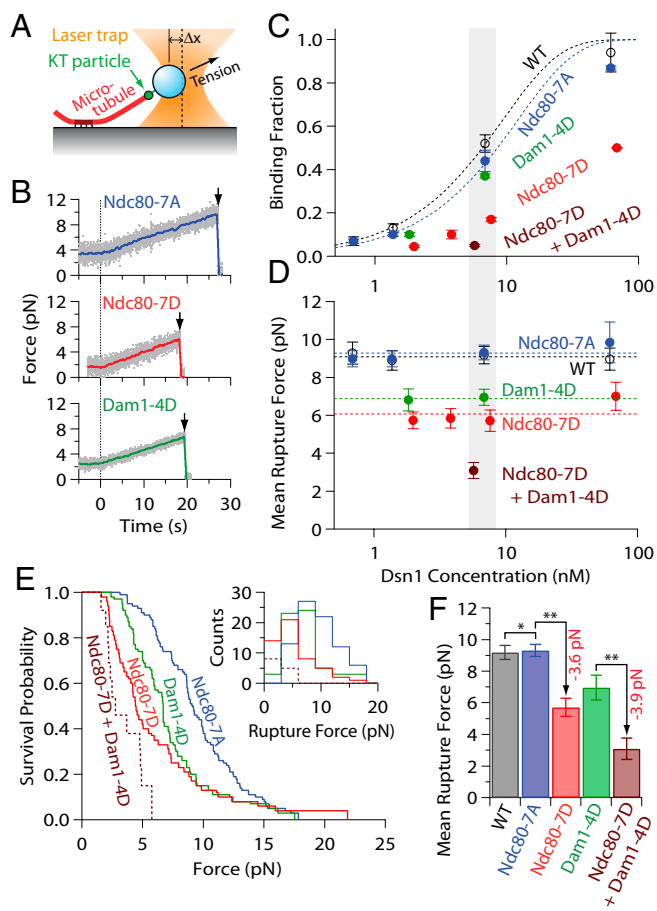


Fig. 2. Phospho-deficient kinetochore particles exhibit wild-type-like rupture strength, phosphomimetics are weaker. (A) Schematic of laser-trap assay. (B) Representative records of tensile force versus time for indicated kinetochore particles bound to assembling tips and then tested with a $0.25 \text{ pN}\cdot\text{s}^{-1}$ force ramp. Gray dots show raw data. Colored traces show the same data after smoothing with a 500-ms sliding boxcar average. Arrows mark ruptures. Dashed vertical lines mark the start of the force ramp. (C) Fraction of beads that bound a growing microtubule tip versus concentration of kinetochore particles used to prepare the beads. Dotted curves show Poisson fits. Error bars represent SD ($n = 2\text{--}20$ experiments) (Table S1). (D) Mean rupture force versus concentration of kinetochore particles used to prepare the beads. (E) Survival probability versus force, and distributions of rupture force (inset), for beads prepared with indicated kinetochore particles at $\sim 6 \text{ nM}$ Dsn1 (which corresponds to the gray shaded regions in C and D). (F) Mean rupture forces for beads prepared at $\sim 6 \text{ nM}$ Dsn1. Error bars in D and F represent SEM ($n = 6\text{--}80$ events) (Table S1). $***P < 0.05$ (statistically significant differences); $*P > 0.1$ (lack of statistical significance). Wild-type data in C, D, and F are from ref. 25.

at various kinetochore densities and across different kinetochore types (Fig. 2 D–F, Figs. S24 and S3, and Table S1).

Phospho-Deficient Kinetochores Behave Like Wild-Type, Phosphomimetics Are Weaker. Previously we found that individual kinetochore particles isolated from asynchronously growing wild-type cells are sufficient for robust tip-coupling with a mean rupture force of $9.1 \pm 0.2 \text{ pN}$ (25). The phosphorylation state of these particles was unknown, but if they carried phosphates at Aurora B target sites, and if these phosphates weakened their tip-coupling strength, then blocking phosphorylation at these sites would be expected to result in higher strength. We found no evidence for such strengthening. Instead, the phospho-deficient Ndc80-7A, Dam1-3A, and Dam1-S20A kinetochore particles all behaved indistinguishably from wild-type, rupturing at $\sim 9 \text{ pN}$ on average

(Fig. 2 D–F and Fig. S3). The mean rupture force for Ndc80-7A, $9.3 \pm 0.4 \text{ pN}$, remained invariant across a 100-fold range of bead decoration densities, overlaying the wild-type data (Fig. 2D). Across this same range, the fraction of active beads varied according to the Poisson probability that the beads carried one or more active kinetochore particles (Fig. 2C and Table S1). These results confirm that, like wild-type particles (25), the phospho-deficient kinetochore particles are sufficient for tip-coupling at the single particle level. The identical strength of wild-type versus phospho-deficient particles suggests that the wild-type particles we tested were not phosphorylated at these Aurora B target sites.

Compared with the phospho-deficient controls, phosphomimetic Ndc80-7D and Dam1-4D kinetochore particles were significantly weaker, rupturing on average at 5.7 ± 0.6 and $7.0 \pm 0.4 \text{ pN}$, respectively (Fig. 2 D–F). Double-mutant Ndc80-7D + Dam1-4D particles carrying both phosphomimetic mutant proteins were even weaker, rupturing at $3.1 \pm 0.4 \text{ pN}$. The reduced strength of these phosphomimetic particles suggests that kinetochore-microtubule attachments can be directly weakened by Aurora B phosphorylation of either Ndc80 or Dam1. Furthermore, the rupture strength of the double-mutant Ndc80-7D + Dam1-4D particles corresponds to a reduction relative to the Ndc80-7A control of $6.2 \pm 0.6 \text{ pN}$, which is very close to the sum of the reductions caused by each set of phosphomimetics alone ($5.9 \pm 0.8 \text{ pN}$), indicating that their effects are additive.

Independent Roles for the Ndc80 and Dam1 Subcomplexes. To further dissect the contributions of Ndc80 and Dam1, we purified kinetochore particles from double-mutants in which *ndc80-7A* or *ndc80-7D* was combined with the temperature-sensitive mutation, *dad1-1*. Kinetochore particles isolated from strains carrying only the *dad1-1* mutation are weaker than wild-type, rupturing at $4.0 \pm 0.4 \text{ pN}$ on average (25), presumably because this mutation disrupts association of the entire Dam1 subcomplex with kinetochores (37). Particles isolated from strains carrying both *ndc80-7A* and *dad1-1* ruptured at $3.8 \pm 0.2 \text{ pN}$, which is statistically indistinguishable from *dad1-1* alone (Fig. S24 and Table S1). Combining *ndc80-7D* with *dad1-1*, however, resulted in further weakening, such that the tip-coupling strength was essentially zero (attachments did not survive the preload period). Notably, the reduction in strength because of Ndc80-7D was roughly equivalent in three different contexts, amounting to -3.6 pN in a wild-type context, -3.9 pN in the context of Dam1-4D, and -3.8 pN in the context of *dad1-1*. This correspondence, together with the additive effects of Ndc80-7D and Dam1-4D, strongly suggests that the Ndc80 subcomplex makes a contribution to tip-coupling strength that is independent of the Dam1 subcomplex.

In vivo, the Ndc80 subcomplex also plays a Dam1-independent role in the initial binding of kinetochores to microtubules (39). We find that this is true in vitro as well. When compared at near-equivalent decoration densities ($\sim 6 \text{ nM}$), the fraction of beads that bound microtubules was significantly lower with Ndc80-7D particles, 0.17 ± 0.01 , than with Ndc80-7A controls, 0.44 ± 0.05 (Fig. S2B and Table S1), or wild-type, 0.52 ± 0.04 (25), demonstrating an important role for Ndc80 in initial binding, and suggesting that this role may be regulated by phosphorylation. In contrast, when decorated with *dad1-1* or Dam1-4D mutant kinetochore particles, the fraction of active beads was much closer to the controls (~ 0.40 , depending on the context). This observation is consistent with previous work showing that initial binding rates in vivo are unaffected by mutations in the Dam1 subcomplex (39). Taken together, our results show that the Ndc80 and Dam1 subcomplexes make distinct contributions to kinetochore particle behavior. The initial binding of the particles to microtubules is dependent mainly on Ndc80 and inhibited by phosphomimetic substitutions on Ndc80. The strength of tip-coupling depends on both Ndc80 and Dam1, and it is reduced by phosphomimetic substitutions on both.

Serine 20 of the Dam1 Protein Is a Key Phospho-Regulatory Site on the Dam1 Subcomplex. Phosphorylation of serine 20 of the Dam1 protein directly weakens the interaction between recombinant Dam1 subcomplexes and taxol-stabilized microtubules (19). Similarly, we found that the single site mutant Dam1-S20D kinetochore particles bound more weakly than wild-type particles to dynamic microtubule tips, rupturing at 7.1 ± 0.6 pN (Fig. S3 and Table S1). This strength is indistinguishable from that of the four-site mutant, Dam1-4D (7.0 ± 0.4 pN), suggesting that the remaining three sites (serines 257, 265, and 292) made no contribution. Indeed, the three-site mutant Dam1-3D particles behaved like wild-type and Ndc80-7A controls, rupturing at ~ 9 pN in force-ramp experiments (Fig. S3 and Table S1). The behavior of Dam1-S20D particles was also indistinguishable from Dam1-4D in force-clamp experiments, which are detailed below. These results highlight the importance of serine 20 of the Dam1 protein for phospho-regulation of kinetochore-microtubule attachment strength. The other three sites are also important *in vivo* (28); but given that phosphomimetics at these sites had no effect in our *in vitro* system, their precise role remains uncertain.

Measuring Kinetochore Detachment Rates and Microtubule Switch Rates Under Constant Tension. We also operated our laser trap in a force-clamp mode, where the bead-trap separation was held constant. This approach allowed us to measure rates of kinetochore detachment during growth and shortening (i.e., k_3 and k_4 in Fig. 1A), and rates of microtubule switching between these two states (“catastrophes” and “rescues,” k_1 and k_2 in Fig. 1A). We studied four kinetochore types, Ndc80-7A, Ndc80-7D, Dam1-4D, and Dam1-S20D, under constant tensile loads of ~ 2.5 pN and at low bead-decoration densities (~ 2 nM Dsn1), well below the single particle limit. All four types maintained persistent, load-bearing attachments to growing and shortening microtubule tips (Fig. 3A), as previously reported for wild-type particles (25). We were unable to study the double-mutant Ndc80-7D + Dam1-4D

with the force clamp, because of its weak rupture strength (Fig. 2D–F and Fig. S24) and very low binding activity (Fig. S2B).

Phosphomimetic Mutations Can Accelerate Detachment and Promote Catastrophe. Average lifetimes for tip attachments mediated by the phosphomimetic Ndc80-7D, Dam1-4D, or Dam1-S20D kinetochore particles, 13.3 ± 2.8 min, 3.3 ± 0.5 min, and 3.0 ± 0.6 min, respectively, were significantly shorter than the Ndc80-7A control, 26.3 ± 6.6 min (Fig. 3D, Fig. S4, and Table S2), consistent with their lower rupture strengths. These same trends were also reflected in detachment rates measured during microtubule growth, which were faster for Ndc80-7D, Dam1-4D, and Dam1-S20D particles (3.5 ± 0.8 h⁻¹, 16.2 ± 2.4 h⁻¹, and 16.9 ± 3.9 h⁻¹, respectively) than for Ndc80-7A (1.3 ± 0.4 h⁻¹) (Fig. 3E, Fig. S4, and Table S3). Taken together, these results support the simple view that kinetochore-microtubule detachment is directly accelerated by Aurora B phosphorylation of either Ndc80 or Dam1.

We also found evidence that Aurora B can promote release by affecting microtubule switch rates. Detachment rates for all four kinetochore types were >10 -fold faster during microtubule shortening (Fig. 3F, Fig. S4, and Table S4) than during growth (Fig. 3E, Fig. S4, and Table S3), indicating that all of the particles were much more vulnerable to detachment during tip shortening, just as we found previously for wild-type particles (25). Given this large difference in stability, any changes in switch rates that cause the microtubule tip to spend more time disassembling can promote kinetochore release indirectly. Indeed, the catastrophe rates for tips attached to phosphomimetic Dam1-4D or Dam1-S20D kinetochore particles, 3.8 ± 1.1 h⁻¹ and 3.6 ± 1.8 h⁻¹, respectively, were threefold higher than for tips attached to Ndc80-7A or Ndc80-7D particles, which switched at ~ 1.3 h⁻¹ (Fig. 3G, Fig. S4, and Table S3). Thus, phosphorylation of the Dam1 subcomplex (but not yeast Ndc80) may promote kinetochore release indirectly, by destabilizing the attached microtubule. A role for Dam1 in stabilizing kinetochore-attached microtubules is consistent with previous

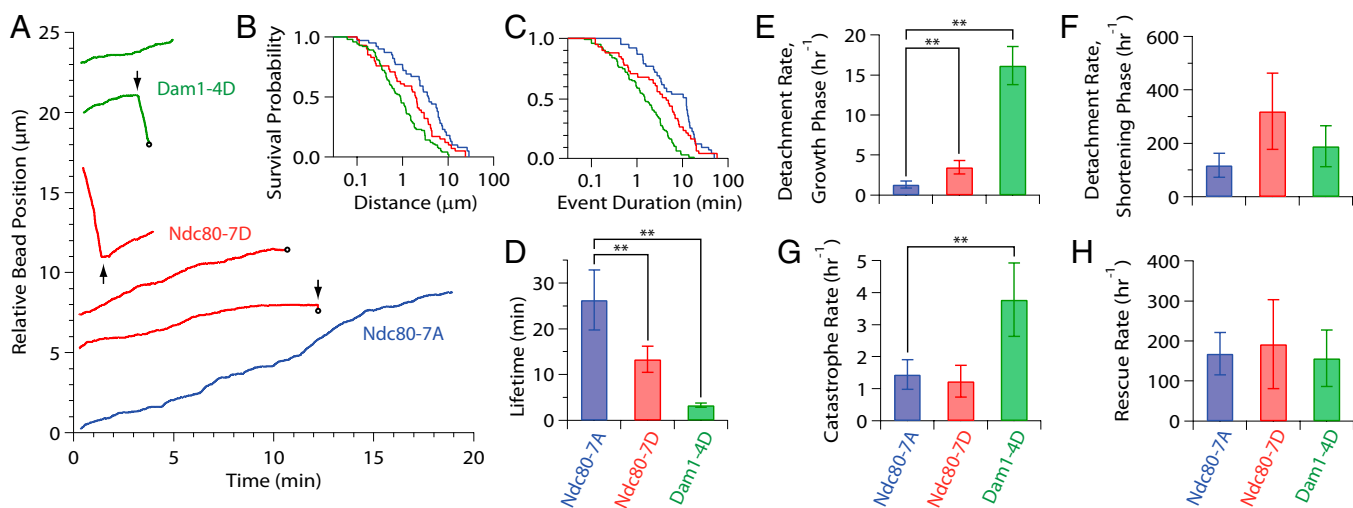


Fig. 3. Phosphomimetic mutations on Dam1 and Ndc80 promote detachment directly and indirectly. (A) Example records of position versus time for Dam1-4D (green, SBY9021), Ndc80-7D (red, SBY8523), and Ndc80-7A (blue, SBY8522) kinetochore particles subjected continuously to 2.5 pN of tension. Increasing position represents movement coupled to microtubule tip growth. Decreasing position represents movement driven by tip shortening. Black arrows indicate catastrophes (↓) and rescues (↑). Black dots indicate detachment of the bead from the microtubule tip. For clarity, traces are offset vertically. (B and C) Survival probability distributions versus total distance traveled (B) and versus event duration (C) for Dam1-4D (green), Ndc80-7D (red), and Ndc80-7A (blue) kinetochore particles. (D) Mean attachment lifetimes for the indicated kinetochore particles under 2.5 pN of tension. Error bars represent uncertainty due to counting statistics ($n = 16$ –53) (Table S2). (E and F) Measured rates of detachment during growth (E) and during shortening (F), corresponding to rates k_3 and k_4 in Fig. 1A, respectively. Error bars represent uncertainty because of counting statistics ($n = 4$ –47) (Tables S3 and S4). (G and H) Measured rates of catastrophe (G) and rescue (H), corresponding to rates k_1 and k_2 in Fig. 1A, respectively. Error bars represent uncertainty because of counting statistics ($n = 3$ –11) (Tables S3 and S4). ** $P < 0.05$ (statistically significant differences) (Table S5). Rates for Dam1-S20D (SBY10280) are given in Tables S2–S4 and Fig. S4.

studies showing that purified Dam1 subcomplex alone promotes microtubule stability (12, 26, 40).

Discussion

Phosphorylation of kinetochores by Aurora B kinase is crucial for correcting erroneous microtubule attachments, but the underlying mechanisms remain unknown. A major impediment has been the difficulty of studying the error-correction process in action. Despite great technical advancements in live imaging (24, 34, 39, 41, 42), it remains very challenging to follow the movements of individual kinetochores in a living cell, to assess whether they are attached to spindle microtubules, and to determine the nature of their attachment (e.g., lateral or tip-attached). To our knowledge, unambiguous kinase-triggered kinetochore detachment events have never been directly observed *in vivo*. Biochemical studies show that the affinity of kinetochore subcomplexes for taxol-stabilized microtubules is reduced by phosphorylation *in vitro*, or by the addition of phosphomimetic mutations at Aurora B target sites. However, assays with artificially stabilized filaments are only rough approximations for the physiological situation, where kinetochores form persistent load-bearing attachments to dynamic microtubule tips. Here we used *in vitro* biophysical methods to measure the strength and stability of attachments between individual dynamic microtubule tips and native kinetochore particles carrying phosphomimetic mutations. Kinetochore detachment was observed directly while growth and shortening of the microtubules was simultaneously recorded, enabling the relationship between phosphoregulation, attachment stability, and filament dynamics to be examined with unprecedented clarity.

Our data suggest that phosphorylation of kinetochores can promote their release from microtubules directly, by accelerating the rate of kinetochore detachment, and also indirectly, by destabilizing the microtubule tip. In principle, both effects could arise simply from a weakening of Ndc80-microtubule and Dam1-microtubule bonds, without major changes in kinetochore particle structure. This view is supported by the weaker binding to microtubules exhibited by individual phosphomimetic Ndc80 subcomplexes (21), and by individual Dam1 subcomplexes phosphorylated at serine 20 (19) versus phospho-deficient controls. Alternatively, phosphorylation may disrupt various bonds within the kinetochore itself, such as Dam1–Dam1 (ring-assembly) interactions (23) or Dam1–Ndc80 interactions (16, 17). Distinguishing among these possibilities will require more precise structural characterization of the phosphomimetic kinetochore particles.

Our results using yeast kinetochore particles are broadly consistent with a recently published study using the human Ndc80 subcomplex alone (21). In either system, phosphomimetic substitutions at Aurora B target sites accelerated detachment rates but also altered microtubule switch rates in a manner that favored tip disassembly. In either system, detachment occurred far more quickly from disassembling versus assembling tips (21). These similarities suggest that the ability of Aurora B to promote kinetochore release both directly and indirectly is conserved from yeast to humans. We note, however, that filament destabilization occurred in a slightly different manner in the two systems. Phosphomimetics on the human Ndc80 subcomplex caused filament

destabilization by lowering the rescue rate for attached microtubule tips. In the yeast system, phosphomimetics on the Dam1 subcomplex caused destabilization by increasing the catastrophe rate. Phosphomimetics on yeast Ndc80 did not appear to affect filament switching, but they accelerated detachment directly. Thus, the overall net effects are similar, but the specific roles of particular phosphorylation sites on particular subcomplexes are somewhat divergent in yeast versus humans.

In all of our *in vitro* work thus far, including studies with Dam1-based, Ndc80-based, and native kinetochore-based couplers, we have seen that attachments made with disassembling tips are less stable than those made with assembling tips (14, 25, 26). If this relationship holds true *in vivo*, it may explain how reactivation of Aurora B, by washout of reversible inhibitors, can promote the correction of erroneous kinetochore-microtubule attachments without necessarily triggering their immediate release (24): Kinetochore phosphorylation may initially trigger disassembly of kinetochore-attached microtubule tips, weakening the kinetochore-microtubule interface but not completely breaking it, but also drawing the kinetochore toward the spindle pole (via disassembly-driven movement). Once near the pole, the interface may then experience higher pulling forces (e.g., because of chromosome crowding or increased “polar ejection”) (43) that are sufficient to cause a complete rupture. A model in which kinetochore phosphoregulation alters microtubule dynamics may also explain why blocking phosphorylation of Ndc80 (Hec1) hyperstabilizes kinetochore-attached microtubule fibers *in vivo* and causes severe defects in chromosome alignment (34, 44).

We chose to focus here on a set of Aurora B target sites within Ndc80 and Dam1 that were most likely to affect kinetochore-microtubule interactions. However, additional sites are also known [e.g., on Ask1 and Spc34 of the Dam1 subcomplex (28), and on Spc105/Knl1 and Dsn1 of the Mtw1/Mis12 subcomplex (22, 45, 46)]. Our approach could be extended to test how phosphoregulation at these other sites promotes kinetochore release. We also consider our measurements of phosphomimetic kinetochore particles to be an important first step toward full reconstitution of Aurora B-triggered kinetochore detachment under load, which will be necessary to understand fully how Aurora B itself is regulated, and how it promotes error correction.

Materials and Methods

Streptavidin-coated polystyrene beads were functionalized with biotinylated anti-His antibodies, decorated with His-tagged kinetochores, and tested against dynamic microtubules grown from GMPCPP-stabilized seeds using a laser trap. Custom control software was used to operate the trap in either a force-ramp or force-clamp mode. Records of bead position and force versus time were recorded using custom LabView software and analyzed using IGOR Pro. Details are provided in *SI Materials and Methods*. See Table S6 for yeast strains used in this study.

ACKNOWLEDGMENTS. We thank Trisha Davis, Matthew Miller, Kwaku Opoku, Jerry Tien, and Neil Umbreit for helpful comments on this manuscript, and members of the Seattle Mitosis Club for helpful discussions. This work was supported by National Institutes of Health Cardiovascular Pathology Traineeship T32HL007312 (to K.K.S.); National Institutes of Health Grant R01GM064386 (to S.B.); and Packard Fellowship 2006-30521 and National Institutes of Health Grant R01GM079373 (to C.L.A.).

- Cheeseman IM, Desai A (2008) Molecular architecture of the kinetochore-microtubule interface. *Nat Rev Mol Cell Biol* 9(1):33–46.
- DeLuca JG, Musacchio A (2012) Structural organization of the kinetochore-microtubule interface. *Curr Opin Cell Biol* 24(1):48–56.
- McAinsh AD, Tytell JD, Sorger PK (2003) Structure, function, and regulation of budding yeast kinetochores. *Annu Rev Cell Dev Biol* 19:519–539.
- Biggins S, et al. (1999) The conserved protein kinase Ipl1 regulates microtubule binding to kinetochores in budding yeast. *Genes Dev* 13(5):532–544.
- Hauf S, et al. (2003) The small molecule Hesperadin reveals a role for Aurora B in correcting kinetochore-microtubule attachment and in maintaining the spindle assembly checkpoint. *J Cell Biol* 161(2):281–294.
- Liu D, Lampson MA (2009) Regulation of kinetochore-microtubule attachments by Aurora B kinase. *Biochem Soc Trans* 37(Pt 5):976–980.
- Tanaka TU, et al. (2002) Evidence that the Ipl1-Sli15 (Aurora kinase-INCENP) complex promotes chromosome bi-orientation by altering kinetochore-spindle pole connections. *Cell* 108(3):317–329.
- Cheeseman IM, Chappie JS, Wilson-Kubalek EM, Desai A (2006) The conserved KMN network constitutes the core microtubule-binding site of the kinetochore. *Cell* 127(5):983–997.
- Hanisch A, Siljé HH, Nigg EA (2006) Timely anaphase onset requires a novel spindle and kinetochore complex comprising Ska1 and Ska2. *EMBO J* 25(23):5504–5515.
- Janke C, Ortiz J, Tanaka TU, Lechner J, Schiebel E (2002) Four new subunits of the Dam1-Duo1 complex reveal novel functions in sister kinetochore biorientation. *EMBO J* 21(1–2):181–193.
- Asbury CL, Gestaut DR, Powers AF, Franck AD, Davis TN (2006) The Dam1 kinetochore complex harnesses microtubule dynamics to produce force and movement. *Proc Natl Acad Sci USA* 103(26):9873–9878.

12. Grishchuk EL, et al. (2008) Different assemblies of the DAM1 complex follow shortening microtubules by distinct mechanisms. *Proc Natl Acad Sci USA* 105(19): 6918–6923.
13. McIntosh JR, et al. (2008) Fibrils connect microtubule tips with kinetochores: A mechanism to couple tubulin dynamics to chromosome motion. *Cell* 135(2):322–333.
14. Powers AF, et al. (2009) The Ndc80 kinetochore complex forms load-bearing attachments to dynamic microtubule tips via biased diffusion. *Cell* 136(5):865–875.
15. Westermann S, et al. (2006) The Dam1 kinetochore ring complex moves processively on depolymerizing microtubule ends. *Nature* 440(7083):565–569.
16. Lampert F, Hornung P, Westermann S (2010) The Dam1 complex confers microtubule plus end-tracking activity to the Ndc80 kinetochore complex. *J Cell Biol* 189(4): 641–649.
17. Tien JF, et al. (2010) Cooperation of the Dam1 and Ndc80 kinetochore complexes enhances microtubule coupling and is regulated by aurora B. *J Cell Biol* 189(4):713–723.
18. Ciferri C, et al. (2008) Implications for kinetochore-microtubule attachment from the structure of an engineered Ndc80 complex. *Cell* 133(3):427–439.
19. Gestaut DR, et al. (2008) Phosphoregulation and depolymerization-driven movement of the Dam1 complex do not require ring formation. *Nat Cell Biol* 10(4):407–414.
20. Alushin GM, et al. (2012) Multimodal microtubule binding by the Ndc80 kinetochore complex. *Nat Struct Mol Biol* 19(11):1161–1167.
21. Umbreit NT, et al. (2012) The Ndc80 kinetochore complex directly modulates microtubule dynamics. *Proc Natl Acad Sci USA* 109(40):16113–16118.
22. Welburn JP, et al. (2010) Aurora B phosphorylates spatially distinct targets to differentially regulate the kinetochore-microtubule interface. *Mol Cell* 38(3):383–392.
23. Wang HW, et al. (2007) Architecture of the Dam1 kinetochore ring complex and implications for microtubule-driven assembly and force-coupling mechanisms. *Nat Struct Mol Biol* 14(8):721–726.
24. Lampson MA, Renduchitala K, Khodjakov A, Kapoor TM (2004) Correcting improper chromosome-spindle attachments during cell division. *Nat Cell Biol* 6(3):232–237.
25. Akiyoshi B, et al. (2010) Tension directly stabilizes reconstituted kinetochore-microtubule attachments. *Nature* 468(7323):576–579.
26. Franck AD, et al. (2007) Tension applied through the Dam1 complex promotes microtubule elongation providing a direct mechanism for length control in mitosis. *Nat Cell Biol* 9(7):832–837.
27. Akiyoshi B, Nelson CR, Ranish JA, Biggins S (2009) Analysis of Ipl1-mediated phosphorylation of the Ndc80 kinetochore protein in *Saccharomyces cerevisiae*. *Genetics* 183(4):1591–1595.
28. Cheeseman IM, et al. (2002) Phospho-regulation of kinetochore-microtubule attachments by the Aurora kinase Ipl1p. *Cell* 111(2):163–172.
29. Guimaraes GJ, Dong Y, McEwen BF, DeLuca JG (2008) Kinetochore-microtubule attachment relies on the disordered N-terminal tail domain of Hec1. *Curr Biol* 18(22): 1778–1784.
30. Miller SA, Johnson ML, Stukenberg PT (2008) Kinetochore attachments require an interaction between unstructured tails on microtubules and Ndc80(Hec1). *Curr Biol* 18(22):1785–1791.
31. Miranda JJ, King DS, Harrison SC (2007) Protein arms in the kinetochore-microtubule interface of the yeast DASH complex. *Mol Biol Cell* 18(7):2503–2510.
32. Ramey VH, et al. (2011) Subunit organization in the Dam1 kinetochore complex and its ring around microtubules. *Mol Biol Cell* 22(22):4335–4342.
33. Wei RR, Al-Bassam J, Harrison SC (2007) The Ndc80/HEC1 complex is a contact point for kinetochore-microtubule attachment. *Nat Struct Mol Biol* 14(1):54–59.
34. DeLuca JG, et al. (2006) Kinetochore microtubule dynamics and attachment stability are regulated by Hec1. *Cell* 127(5):969–982.
35. Keating P, Rachidi N, Tanaka TU, Stark MJ (2009) Ipl1-dependent phosphorylation of Dam1 is reduced by tension applied on kinetochores. *J Cell Sci* 122(Pt 23): 4375–4382.
36. Tooley JG, Miller SA, Stukenberg PT (2011) The Ndc80 complex uses a tripartite attachment point to couple microtubule depolymerization to chromosome movement. *Mol Biol Cell* 22(8):1217–1226.
37. Enquist-Newman M, et al. (2001) Dad1p, third component of the Duo1p/Dam1p complex involved in kinetochore function and mitotic spindle integrity. *Mol Biol Cell* 12(9):2601–2613.
38. Franck AD, Powers AF, Gestaut DR, Davis TN, Asbury CL (2010) Direct physical study of kinetochore-microtubule interactions by reconstitution and interrogation with an optical force clamp. *Methods* 51(2):242–250.
39. Tanaka K, et al. (2005) Molecular mechanisms of kinetochore capture by spindle microtubules. *Nature* 434(7036):987–994.
40. Westermann S, et al. (2005) Formation of a dynamic kinetochore-microtubule interface through assembly of the Dam1 ring complex. *Mol Cell* 17(2):277–290.
41. Dewar H, Tanaka K, Nasmyth K, Tanaka TU (2004) Tension between two kinetochores suffices for their bi-orientation on the mitotic spindle. *Nature* 428(6978):93–97.
42. Magidson V, et al. (2011) The spatial arrangement of chromosomes during prometaphase facilitates spindle assembly. *Cell* 146(4):555–567.
43. Rieder CL, Salmon ED (1994) Motile kinetochores and polar ejection forces dictate chromosome position on the vertebrate mitotic spindle. *J Cell Biol* 124(3):223–233.
44. DeLuca KF, Lens SM, DeLuca JG (2011) Temporal changes in Hec1 phosphorylation control kinetochore-microtubule attachment stability during mitosis. *J Cell Sci* 124(Pt 4):622–634.
45. Maskell DP, Hu XW, Singleton MR (2010) Molecular architecture and assembly of the yeast kinetochore MIND complex. *J Cell Biol* 190(5):823–834.
46. Westermann S, et al. (2003) Architecture of the budding yeast kinetochore reveals a conserved molecular core. *J Cell Biol* 163(2):215–222.

Supporting Information

Sarangapani et al. 10.1073/pnas.1220700110

SI Materials and Methods

Isolation of Kinetochores Particles. Kinetochores particles were isolated by affinity-purifying Dsn1-His-Flag protein using a previously-described minichromosome purification protocol (1) but with some modifications. The Ndc80-7A, Ndc80-7D, and Ndc80-WT kinetochores particles were purified from asynchronously growing cells. The Dam1 phosphomutants and all of the Ndc80 + Dam1 double mutants were purified from cells arrested in media containing benomyl to ensure that they were in the same cell-cycle stage. For benomyl arrest, YPD media containing 120 $\mu\text{g}/\text{mL}$ benomyl was prepared by adding benomyl (30 mg/mL stock solution dissolved in DMSO) to boiling media and cooled to room temperature. Equivalent amounts of benomyl media were added to growing cell cultures (at $\text{OD}_{600} \sim 0.7$) so that the final benomyl concentration was 60 $\mu\text{g}/\text{mL}$. Cells were grown for an additional 3 h and harvested when greater than 90% of cells were large-budded. For both asynchronously growing and benomyl-arrested cultures, 1–5 L of cells were harvested and extract was prepared by breaking cells in a blender with dry ice, followed by ultracentrifugation. Beads conjugated with anti-Flag antibodies were incubated with extract for 3 h with constant rotation, followed by four washes with BH/0.15 [25 mM Hepes pH 8.0, 2 mM MgCl_2 , 0.1 mM EDTA pH 8.0, 0.5 mM EGTA pH 8.0, 0.1% Nonidet P-40, 150 mM KCl, 15% (vol/vol) glycerol] containing protease inhibitors, phosphatase inhibitors, and 2 mM DTT. Beads were further washed twice with BH/0.15 with protease inhibitors. Associated proteins were eluted from the beads by gentle agitation of beads in elution buffer (0.5 mg/mL 3FLAG peptide in BH/0.15 with protease inhibitors) for 25 min at room temperature. Typical concentrations of Dsn1-His-Flag ranged between 1.5 and 4.5 $\mu\text{g}/\text{mL}$ (20–60 nM Dsn1) as determined by comparing the purified material with BSA standards on silver-stained SDS/PAGE gels. Aliquots were made and stored at -80°C .

Laser-Trap Instrument. The instrument has been described previously (2). Position sensor response was mapped using the piezo stage to raster-scan a stuck bead through the beam, and trap stiffness was calibrated along the two principle axes using the drag force, equipartition, and power spectrum methods. Force feedback was implemented with custom LabView software. During force measurements, bead-trap separation was sampled at 40 kHz; stage position was updated at 50 Hz to maintain the desired tension (force-clamp assay) or ramp-rate (force-ramp assay). Bead and stage position data were decimated to 0.2 kHz before storing to disk.

Rupture Force Measurements. Native kinetochores particles were linked to beads as previously described (3). Streptavidin-coated polystyrene beads (0.44 μm in diameter; Spherotech) were functionalized with biotinylated anti-His₅ antibodies (Qiagen) and stored with continuous rotation at 4°C in BRB80 (80 mM Pipes, 1 mM MgCl_2 , and 1 mM EGTA, pH 6.9) supplemented with 8 $\text{mg}\cdot\text{mL}^{-1}$ BSA for up to 3 mo. Immediately before each experiment, beads were decorated with kinetochores particles by incubating 6 pM anti-His₅ beads for 60 min at 4°C with different amounts of the purified kinetochores material, corresponding to Dsn1-His-Flag concentrations ranging from 0.6 to 70 nM. Flow chambers ($\sim 10\text{-}\mu\text{L}$ volume) were constructed and functionalized as previously described (2). First, 10 μL of 10 $\text{mg}\cdot\text{mL}^{-1}$ biotinylated BSA (Vector Laboratories) was introduced and allowed to bind to the glass surface for 15 min at room temperature. The chamber was then washed with 100 μL of BRB80. Next, 75–100 μL

of 0.33 $\text{mg}\cdot\text{mL}^{-1}$ avidin DN (Vector Laboratories) was introduced, incubated for 3 min, and washed out with 100 μL of BRB80. GMPCPP-stabilized biotinylated microtubule seeds were introduced in BRB80, and allowed to bind to the functionalized glass surface for 3 min. The chamber was then washed with 100 μL of growth buffer (BRB80 containing 1 mM GTP and 1 $\text{mg}\cdot\text{mL}^{-1}$ κ -casein). Finally, kinetochores particle-coated beads were introduced at an eightfold dilution from the incubation mix (see above) in a solution of growth buffer containing 1.5 $\text{mg}\cdot\text{mL}^{-1}$ purified bovine brain tubulin, 1 mM DTT, 500 $\mu\text{g}\cdot\text{mL}^{-1}$ glucose oxidase, 60 $\mu\text{g}\cdot\text{mL}^{-1}$ catalase, and 25 mM glucose. The edges of the flow chamber were sealed with nail polish to prevent evaporation. All laser-trap experiments were performed at 23°C .

Using the laser trap, individual beads were attached to the ends of growing microtubules and preloaded with a constant force ranging between 2 and 4 pN. After a brief preload period, during which we verified that the beads were moving at a rate consistent with that of microtubule growth, the laser trap was programmed to ramp the force at a constant rate (0.25 $\text{pN}\cdot\text{s}^{-1}$) until the linkage ruptured, or until the load limit of the trap (~ 20 pN) was reached and the bead escaped from the trap. At all Dsn1-His-Flag concentrations below 60 nM, the fraction of beads that reached the load limit and escaped the trap was small (10–15%). Because only 1–2 min was required to record each individual rupture event, large populations could be measured relatively efficiently, facilitating statistical analysis. Statistics for this dataset are given in Table S1.

Force-Clamp Assay. Kinetochores-decorated beads were prepared as described above using a Dsn1:bead ratio of 200:1 (~ 2 nM Dsn1-His-Flag; 5.6-pM beads), which is well below the single particle limit (3). The beads were introduced into a flow cell, attached to the ends of growing microtubules, and subjected to tensile force as described above, except that the laser trap was programmed to maintain a constant mean force, ~ 2.5 pN. Statistics for this dataset are shown in Tables S2–S5. Attachment lifetimes were computed from the instant an attachment was fully loaded until the event ended, often because of bead detachment but sometimes for other reasons (e.g., when another bead fell into the trap). All individual event durations were considered, irrespective of how the events ended. Lifetimes (Fig. 3D) were computed by summing the total time of all events and dividing by the number of detachments. The rate of detachment during growth (Fig. 3E) and the catastrophe rate (Fig. 3G) were computed by counting the numbers of these events and dividing by the total microtubule assembly (growth) time. Similarly, the rates of detachment during shortening (Fig. 3F) and the rescue rate (Fig. 3H) were computed by counting events and dividing by the total microtubule disassembly (shortening) time.

Statistical Analyses. The P values for comparison of mean rupture forces (Fig. 2F, and Figs. S2A and S3) were computed by single-factor ANOVA. For the data in Fig. 3, we computed the P values from their corresponding z -scores, given by $z = (\mu_1 - \mu_2) \cdot (\delta_1^2 + \delta_2^2)^{-0.5}$. Here, μ_1 and μ_2 are the means of any given parameter (e.g., lifetime, catastrophe rate, and so forth) for the two molecular systems being compared (e.g., Ndc80-7A, or Dam1-4D) and δ_1 and δ_2 are the corresponding errors based on counting statistics, as detailed in Tables S2–S5. The z -score denotes how many SDs separate the two mean values and allows the statistical significance (or lack thereof) of their separation to be estimated.

Contributions of the Ndc80 Subcomplex to Both Initial Binding and Tip-Coupling. Across eukaryotes, kinetochore-microtubule coupling depends on the Ndc80 subcomplex, but its exact role in yeast remains a subject of discussion. Studies in metazoans suggest that kinetochore-anchored Ndc80 subcomplexes provide direct microtubule interactions that represent the primary microtubule attachment interface (4, 5). Consistent with this view, truncation of the N-terminal Ndc80 tail, which dramatically reduces its microtubule binding affinity *in vitro* (6–9), also severely destabilizes kinetochore-microtubule attachments in metazoan cells (10–13). However, yeast survive truncation of the Ndc80 tail (14, 15), and it has been suggested that Ndc80 in yeast may instead act mainly as a scaffold onto which other microtubule-binding subcomplexes, such as Dam1, must assemble to form the primary interface (16). In our view, the idea that yeast

Ndc80 acts solely as a scaffold is difficult to reconcile with the available data. Yeast kinetochores make initial, Ndc80-dependent lateral attachments to microtubules even when the Dam1 complex is disrupted, both *in vivo* (17) and also *in vitro* (Fig. S2B) (3). Phosphomimetic mutations on Ndc80 also weaken the tip-coupling strength of yeast kinetochore particles by an equivalent amount, regardless of the state of the Dam1 complex (Fig. 3F and Fig. S2A). Thus, Ndc80 makes contributions to initial attachment, and also to tip-coupling strength, that appear to be independent of Dam1. Moreover, tail truncation does not completely abolish the affinity of Ndc80 for microtubules (6–9, 18). Thus, the viability of yeast lacking the tail of Ndc80 probably reflects a difference in the degree to which they rely on the tail, or a functional redundancy between the Ndc80 and Dam1 complexes (14, 18), rather than a fundamental difference in the role of Ndc80.

1. Akiyoshi B, Nelson CR, Ranish JA, Biggins S (2009) Quantitative proteomic analysis of purified yeast kinetochores identifies a PP1 regulatory subunit. *Genes Dev* 23(24):2887–2899.
2. Franck AD, Powers AF, Gestaut DR, Davis TN, Asbury CL (2010) Direct physical study of kinetochore-microtubule interactions by reconstitution and interrogation with an optical force clamp. *Methods* 51(2):242–250.
3. Akiyoshi B, et al. (2010) Tension directly stabilizes reconstituted kinetochore-microtubule attachments. *Nature* 468(7323):576–579.
4. Cheeseman IM, Desai A (2008) Molecular architecture of the kinetochore-microtubule interface. *Nat Rev Mol Cell Biol* 9(1):33–46.
5. DeLuca JG, Musacchio A (2012) Structural organization of the kinetochore-microtubule interface. *Curr Opin Cell Biol* 24(1):48–56.
6. Alushin GM, et al. (2012) Multimodal microtubule binding by the Ndc80 kinetochore complex. *Nat Struct Mol Biol* 19(11):1161–1167.
7. Ciferri C, et al. (2008) Implications for kinetochore-microtubule attachment from the structure of an engineered Ndc80 complex. *Cell* 133(3):427–439.
8. Umbreit NT, et al. (2012) The Ndc80 kinetochore complex directly modulates microtubule dynamics. *Proc Natl Acad Sci USA* 109(40):16113–16118.
9. Wei RR, Al-Bassam J, Harrison SC (2007) The Ndc80/HEC1 complex is a contact point for kinetochore-microtubule attachment. *Nat Struct Mol Biol* 14(1):54–59.
10. DeLuca JG, et al. (2005) Hec1 and nuf2 are core components of the kinetochore outer plate essential for organizing microtubule attachment sites. *Mol Biol Cell* 16(2):519–531.
11. DeLuca JG, Moree B, Hickey JM, Kilmartin JV, Salmon ED (2002) hNuf2 inhibition blocks stable kinetochore-microtubule attachment and induces mitotic cell death in HeLa cells. *J Cell Biol* 159(4):549–555.
12. Guimaraes GJ, Dong Y, McEwen BF, DeLuca JG (2008) Kinetochore-microtubule attachment relies on the disordered N-terminal tail domain of Hec1. *Curr Biol* 18(22):1778–1784.
13. McClelland ML, et al. (2003) The highly conserved Ndc80 complex is required for kinetochore assembly, chromosome congression, and spindle checkpoint activity. *Genes Dev* 17(1):101–114.
14. Demirel PB, Keyes BE, Chatterjee M, Remington CE, Burke DJ (2012) A redundant function for the N-terminal tail of Ndc80 in kinetochore-microtubule interaction in *Saccharomyces cerevisiae*. *Genetics* 192(2):753–756.
15. Kemmler S, et al. (2009) Mimicking Ndc80 phosphorylation triggers spindle assembly checkpoint signalling. *EMBO J* 28(8):1099–1110.
16. Lampert F, Hornung P, Westermann S (2010) The Dam1 complex confers microtubule plus end-tracking activity to the Ndc80 kinetochore complex. *J Cell Biol* 189(4):641–649.
17. Tanaka K, et al. (2005) Molecular mechanisms of kinetochore capture by spindle microtubules. *Nature* 434(7036):987–994.
18. Lampert F, Mieck C, Alushin GM, Nogales E, Westermann S (2013) Molecular requirements for the formation of a kinetochore-microtubule interface by Dam1 and Ndc80 complexes. *J Cell Biol* 200:21–30.

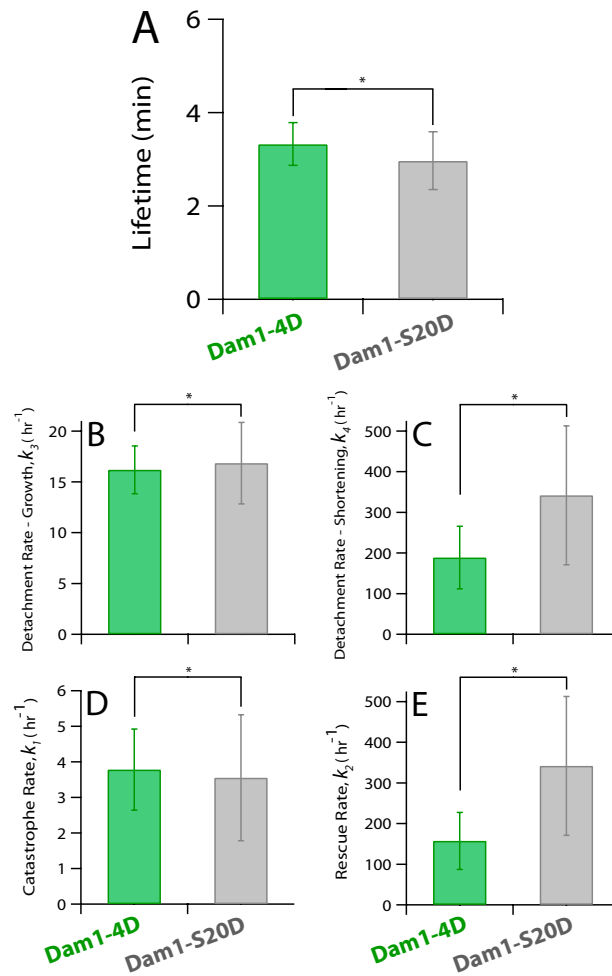


Fig. S4. Additional evidence that serine 20 of the Dam1 protein is a key phospho-regulatory site. Data from the force-clamp experiments of Figs. 3 *D–H* for the four-site phosphomimetic Dam1-4D are replotted here (green bars), together with the attachment lifetime (A), detachment rate during growth (B), detachment rate during shortening (C), catastrophe rate (D), and rescue rate (E) for the one-site phosphomimetic, Dam1-S20D (gray bars, SBY10280). The force-clamp behavior of Dam1-S20D is indistinguishable from that of Dam1-4D (SBY9021), as we also found in force-ramp experiments (Fig. S3). Error bars represent uncertainty due to counting statistics. * $P > 0.1$ (lack of statistical significance).

Table S1. Statistics for rupture force experiments

Kinetochores	~1nM (0.6–2 nM) Dsn1		~2 nM (1–4 nM) Dsn1		~6 nM (6–8 nM) Dsn1		~65 nM (60–70 nM) Dsn1	
	Binding fraction	Rupture force (pN)	Binding fraction	Rupture force (pN)	Binding fraction	Rupture force (pN)	Binding fraction	Rupture force (pN)
Wild-type*	0.07 ± 0.02 (n = 6)	9.29 ± 0.58 (n = 43)	0.13 ± 0.02 (n = 7)	8.90 ± 0.51 (n = 64)	0.52 ± 0.04 (n = 7)	9.18 ± 0.45 (n = 70)	0.94 ± 0.09 (n = 4)	8.97 ± 0.59 (n = 47)
Ndc80-WT [†]					0.41 ± 0.07 (n = 2)	8.32 ± 0.48 (n = 50)		
Ndc80-7A	0.07 ± 0.01 (n = 4)	8.99 ± 0.42 (n = 62)	0.10 ± 0.01 (n = 12)	8.98 ± 0.42 (n = 55)	0.44 ± 0.05 (n = 3)	9.31 ± 0.38 (n = 80)	0.87 ± 0.01 (n = 2)	9.85 ± 1.08 (n = 6)
Ndc80-7D	0.045 ± 0.004 (n = 2)	5.73 ± 0.44 (n = 42)	0.10 ± 0.02 (n = 20)	5.84 ± 0.51 (n = 42)	0.17 ± 0.01 (n = 3)	5.71 ± 0.57 (n = 52)	0.50 ± 0.01 (n = 2)	7.01 ± 0.74 (n = 34)
Dam1-4A	No data available because these cells are inviable [‡]							
Dam1-4D			0.10 ± 0.01 (n = 9)	6.82 ± 0.59 (n = 36)	0.37 ± 0.01 (n = 2)	6.96 ± 0.42 (n = 42)		
Ndc80-7D + Dam1-4D					0.05 ± 0.004 (n = 2)	3.09 ± 0.42 (n = 13)		
Dam1-3A					0.47 ± 0.04 (n = 2)	9.33 ± 0.79 (n = 29)		
Dam1-3D					0.55 ± 0.05 (n = 2)	9.87 ± 0.67 (n = 26)		
Dam1-S20A					0.48 ± 0.03 (n = 3)	9.35 ± 0.57 (n = 45)		
Dam1-S20D			0.10 ± 0.01 (n = 4)		0.48 ± 0.08 (n = 2)	7.12 ± 0.61 (n = 31)		
<i>dad1-1</i> *					0.40 ± 0.05 (n = 6)	3.97 ± 0.37 (n = 60)		
Ndc80-7A + <i>dad1-1</i>					0.48 ± 0.07 (n = 3)	3.75 ± 0.23 (n = 57)		
Ndc80-7D + <i>dad1-1</i>					0.02 ± 0.02 (n = 2)	–0–		

Binding fractions indicate the proportion of beads that bound when held near the tip of a growing microtubule, expressed as mean ± SD from *n* experiments. The number of individual beads tested during each experiment ranged from 5 to 50. Rupture forces indicate mean ± SEM from *n* individual rupture events. The Dsn1 concentrations used for bead decoration were slightly different for the various mutants, and are grouped here into four categories with mean values (~) and ranges indicated. The colors for kinetochores types Ndc80-7A (blue), Ndc80-7D (red), Dam1-4D (green), and Ndc80-7D + Dam1-4D (brown) were chosen to match those in Figs. 2 and 3, and Figs. S2–S4.

*Published previously in Akiyoshi et al. (1).

[†]Wild-type Ndc80 integrated at a different locus (SBY8524), as a control for Ndc80-7A and Ndc80-7D mutants.

[‡]Ref. 2.

1. Akiyoshi B, et al. (2010) Tension directly stabilizes reconstituted kinetochore-microtubule attachments. *Nature* 468(7323):576–579.

2. Cheeseman IM, et al. (2002) Phospho-regulation of kinetochore-microtubule attachments by the Aurora kinase Ipl1p. *Cell* 111(2):163–172.

Table S2. Statistics for force-clamp (constant force) experiments: Total lifetimes

Kinetochores	Mean clamp force ± error (pN)	Total no. detachments	Lifetime ± error (min)
Ndc80-7A	2.57 ± 0.62	16	26.28 ± 6.57
Ndc80-7D	2.58 ± 0.55	22	13.31 ± 2.83
Dam1-4D	2.36 ± 1.41	53	3.33 ± 0.46
Dam1-S20D	1.88 ± 1.48	23	2.97 ± 0.62

To calculate mean attachment lifetimes, the total time (spent in growth and shortening) was divided by the total number of detachments (from growing or shortening microtubules). Estimated errors represent uncertainty because of counting statistics, which were computed as $\delta = \mu \cdot N^{-1} \sqrt{N}$, where μ is the mean rate (or lifetime) and $N^{-1} \sqrt{N}$ is the fractional uncertainty. The colors for kinetochores types Ndc80-7A (blue), Ndc80-7D (red), and Dam1-4D (green) were chosen to match those in Figs. 2 and 3 and Figs. S2–S4.

Table S3. Statistics for force-clamp (constant force) experiments: Growing tips

Kinetochores	Mean clamp force \pm error (pN)	No. detachments (growing tips)	Total growth time (h)	Detachment rate, growth \pm error (h^{-1})	No. catastrophes	Catastrophe rate \pm error (h^{-1})
Ndc80-7A	2.57 \pm 0.62	9	6.95	1.30 \pm 0.43	10	1.44 \pm 0.46
Ndc80-7D	2.58 \pm 0.55	17	4.86	3.50 \pm 0.85	6	1.23 \pm 0.50
Dam1-4D	2.36 \pm 1.41	47	2.91	16.18 \pm 2.36	11	3.78 \pm 1.14
Dam1-S20D	1.88 \pm 1.48	19	1.13	16.85 \pm 3.87	4	3.55 \pm 1.77

Mean rates for detachment from growing microtubules and for catastrophe were calculated by dividing the number of events by the total observed growth time. Estimated errors represent uncertainty because of counting statistics, which were computed as $\delta = \mu \cdot N^{-1} \sqrt{N}$, where μ is the mean rate (or lifetime) and $N^{-1} \sqrt{N}$ is the fractional uncertainty. The colors for kinetochore types Ndc80-7A (blue), Ndc80-7D (red), and Dam1-4D (green) were chosen to match those in Figs. 2 and 3 and Figs. S2–S4.

Table S4. Statistics for force-clamp (constant force) experiments: Shortening tips

Kinetochores	Mean clamp force \pm error (pN)	No. detachments (shortening tips)	Total shortening time (h)	Detachment rate, shortening \pm error (h^{-1})	No. rescues	Rescue rate \pm error (h^{-1})
Ndc80-7A	2.57 \pm 0.62	7	0.060	117.62 \pm 44.46	10	168.03 \pm 53.14
Ndc80-7D	2.58 \pm 0.55	5	0.016	320.34 \pm 143.26	3	192.21 \pm 110.97
Dam1-4D	2.36 \pm 1.41	6	0.032	188.55 \pm 76.97	5	157.12 \pm 70.27
Dam1-S20D	1.88 \pm 1.48	4	0.012	341.76 \pm 170.88	4	341.76 \pm 170.88

Mean rates for detachment from shortening microtubules and for rescue were calculated by dividing the number of events by the total observed shortening time. Estimated errors represent uncertainty because of counting statistics, which were computed as $\delta = \mu \cdot N^{-1} \sqrt{N}$, where μ is the mean rate (or lifetime) and $N^{-1} \sqrt{N}$ is the fractional uncertainty. The colors for kinetochore types Ndc80-7A (blue), Ndc80-7D (red), and Dam1-4D (green) were chosen to match those in Figs. 2 and 3 and Figs. S2–S4.

Table S5. Statistics for force-clamp (constant force) experiments: P values

Kinetochores compared	P value				
	Lifetime	Detachment rate, growth	Detachment rate, shortening	Catastrophe rate	Rescue rate
Ndc80-7A vs. Ndc80-7D	0.02**	0.04**	0.12*	0.39*	0.19*
Ndc80-7A vs. Dam1-4D	0.0001**	0**	0.21*	0.03**	0.33*
Dam1-4D vs. Dam1-S20D	0.68*	0.54*	0.16*	0.44*	0.79*

The colors for kinetochore types Ndc80-7A (blue), Ndc80-7D (red), and Dam1-4D (green) were chosen to match those in Figs. 2 and 3 and Figs. S2–S4. Statistically significant differences are shown in boldface. P values were calculated from z-scores, as detailed in *SI Materials and Methods*. ** $P < 0.05$; * $P > 0.1$.

Table S6. Yeast strains used in this study

Strain	Genotype
SBY8253	<i>MATa ura3-1 leu2,3-112 his3-11 trp1-1 ade2-1 LYS2 can1-100 bar1-1 DSN1-6HIS-3FLAG::URA3</i>
SBY8460	<i>MATa ura3-1 leu2,3-112 his3-11 trp1-1::256lacO::TRP1 ade2-1 can1-100 LYS2 bar1-1 DSN1-6HIS-3FLAG::URA3 dad1-1::KAN</i>
SBY8522	<i>MATa ura3-1 leu2,3-112 his3-11 trp1-1 ade2-1 LYS2 can1-100 bar1-1 DSN1-6HIS-3FLAG::URA3 ndc80::NAT::ndc80(T21A,S37A,T54A,T71A,T74A,S95A,S100A)::TRP1</i>
SBY8523	<i>MATa ura3-1 leu2,3-112 his3-11 trp1-1 ade2-1 LYS2 can1-100 bar1-1 DSN1-6HIS-3FLAG::URA3 ndc80::NAT::ndc80(T21E,S37D,T54E,T71E,T74E,S95D,S100E)::TRP1</i>
SBY8524	<i>MATa ura3-1 leu2,3-112 his3-11 trp1-1 ade2-1 LYS2 can1-100 bar1-1 DSN1-6HIS-3FLAG::URA3 ndc80::NAT::NDC80::TRP1</i>
SBY9020	<i>MATa ura3-1 leu2,3-112 his3-11 trp1-1 ade2-1 lys2Δ can1-100 bar1-1 DSN1-6HIS-3FLAG::URA3 ndc80::NAT::ndc80(T21E,S37D,T54E,T71E,T74E,S95D,S100E)::TRP1 dam1(S20D,S257D,S265D,S292D)::KanMX</i>
SBY9021	<i>MATa ura3-1 leu2,3-112 his3-11 trp1-1 ade2-1 lys2Δ can1-100 bar1-1 DSN1-6HIS-3FLAG::URA3 dam1(S20D,S257D,S265D,S292D)::KanMX</i>
SBY9469	<i>MATa ura3-1 leu2,3-112 his3-11 trp1-1::256lacO::TRP1 ade2-1 LYS2 can1-100 bar1-1 DSN1-6HIS-3FLAG::URA3 dad1-1::KanMX ndc80::NAT::ndc80(T21A,S37A,T54A,T71A,T74A,S95A,S100A)::TRP1</i>
SBY9470	<i>MATa ura3-1 leu2,3-112 his3-11 trp1-1::256lacO::TRP1 ade2-1 LYS2 can1-100 bar1-1 DSN1-6HIS-3FLAG::URA3 dad1-1::KanMX ndc80::NAT::ndc80(T21E,S37D,T54E,T71E,T74E,S95D,S100E)::TRP1</i>
SBY9471	<i>MATa ura3-1 leu2,3-112 his3-11 trp1-1::256lacO::TRP1 ade2-1 LYS2 can1-100 bar1-1 DSN1-6HIS-3FLAG::URA3 dad1-1::KanMX ndc80::NAT::NDC80::TRP1</i>
SBY10278	<i>MATa ura3-1 leu2,3-112 his3-11 trp1-1 ade2-1 LYS2 can1-100 bar1-1 DSN1-6HIS-3FLAG::URA3 dam1(S20A)::KanMX</i>
SBY10280	<i>MATa ura3-1 leu2,3-112 his3-11 trp1-1 ade2-1 LYS2 can1-100 bar1-1 DSN1-6HIS-3FLAG::URA3 dam1(S20D)::KanMX</i>
SBY10342	<i>MATa ura3-1 leu2,3-112 his3-11 trp1-1 ade2-1 LYS2 can1-100 bar1-1 DSN1-6HIS-3FLAG::URA3 dam1(S257D,S265D,S292D)::KanMX</i>
SBY10457	<i>MATa ura3-1 leu2,3-112 his3-11 trp1-1 ade2-1 LYS2 can1-100 bar1-1 DSN1-6HIS-3FLAG::URA3 dam1(S257A,S265A,S292A)::KanMX</i>

All strains are isogenic with the W303 background. The *Ndc80-7D* (T21E,S37D,T54E,T71E,T74E,S95D,S100E) strain was made as described in ref. 1 and shows no obvious growth defect in vivo.

1. Akiyoshi B, Nelson CR, Ranish JA, Biggins S (2009) Analysis of Ipl1-mediated phosphorylation of the Ndc80 kinetochore protein in *Saccharomyces cerevisiae*. *Genetics* 183(4):1591–1595.